J|A|C|S
ARTICLES
Published on Web 08/15/2006

# Chemical Shift Tensors of Protonated Base Carbons in Helical RNA and DNA from NMR Relaxation and Liquid Crystal Measurements

Jinfa Ying,*,† Alexander Grishaev,*,† David L. Bryce,*,‡ and Ad Bax*,†

*Contribution from the Laboratory of Chemical Physics, National Institute of Diabetes and Digestive and Kidney Diseases, National Institutes of Health, Bethesda, Maryland 20892, and Department of Chemistry, University of Ottawa, Ottawa, Ontario K1N 6N5, Canada*

Received March 22, 2006; E-mail: jinfaying@niddk.nih.gov; alexanderg@intra.niddk.nih.gov; dbryce@uottawa.ca; bax@nih.gov

***Abstract:*** Knowledge of $^{13}C$ chemical shift anisotropy (CSA) tensors in nucleotide bases is important for interpretation of NMR relaxation data in terms of local dynamic properties of nucleic acids and for analysis of residual chemical shift anisotropy (RCSA) resulting from weak alignment. CSA tensors for protonated nucleic acid base carbons have been derived from measurements on a uniformly $^{13}C$-enriched helical A-form RNA segment and a helical B-form DNA dodecamer at natural $^{13}C$ abundance. The magnitudes of the derived CSA principal values are tightly restricted by the magnetic field dependencies of the $^{13}C$ transverse relaxation rates, whereas the tensor orientation and asymmetry follow from quantitative measurements of interference between $^{13}C$-{$^{1}H$} dipolar and $^{13}C$ CSA relaxation mechanisms. Changes in the chemical shift between the isotropic and aligned states, $\Delta\delta$, complement these measurements and permit cross-validation. The CSA tensors are determined from the experimental $\Delta\delta$ values and relaxation rates, under the assumption that the CSA tensor of any specific carbon in a given type of base is independent of the base position in either the RNA or DNA helix. However, the experimental data indicate that for pyrimidine $C_6$ carbons in A-form RNA the CSA magnitude is considerably larger than in B-form DNA. This result is supported by quantum chemical calculations and is attributed in part to the close proximity between intranucleotide $C_6H$ and $O_5'$ atoms in RNA. The magnitudes of the measured CSA tensors, on average, agree better with previous solid-state NMR results obtained on powdered nucleosides than with prior results from quantum chemical calculations on isolated bases, which depend rather strongly on the level of theory at which the calculations are carried out. In contrast, previously computed orientations of the chemical shift tensors agree well with the present experimental results and exhibit less dependence on the level of theory at which the computations are performed.

## Introduction

The study of the structure of nucleic acids by NMR spectroscopy has mostly relied upon semiquantitative local restraints such as NOEs and *J* couplings.[1] However, the paucity of useful long-range NOE data in such molecules can make accurate structure determination particularly challenging because small local uncertainties rapidly propagate and cause large uncertainties in global features such as helix bending or relative helix orientations.[2−4] Weak alignment of DNA and RNA in the magnetic field, in combination with isotopic enrichment procedures, has made the measurement of residual dipolar couplings (RDCs), which define individual bond vector orientations relative to the molecule's alignment frame, possible. Because the vector orientations are derived relative to a single alignment frame, rather than relative to one another, they are often referred to as "global" restraints and provide an ideal complement to the local structural information contained in NOEs and *J* couplings. This makes it possible to accurately determine properties such as helix bending and relative orientation of structural elements.[5−11] RDC measurements typically are made by dissolving the nucleic acid in a liquid crystalline aligning medium,[12−14] by soaking it into a hydrogel that is subsequently anisotropically compressed,[15−17] or simply by taking advantage

† National Institutes of Health.
‡ University of Ottawa.

(1) Wüthrich, K. *NMR of Proteins and Nucleic Acids*; John Wiley & Sons: New York, 1986.
(2) Metzler, W.; Wang, C.; Kitchen, D.; Levy, R.; Pardi, A. *J. Mol. Biol.* **1990**, *214*, 711−736.
(3) Ulyanov, N. B.; Gorin, A. A.; Zhurkin, V. B.; Chen, B. C.; Sarma, M. H.; Sarma, R. H. *Biochemistry* **1992**, *31*, 3918−3930.
(4) Allain, F. H. T.; Varani, G. *J. Mol. Biol.* **1997**, *267*, 338−351.
(5) Mollova, E. T.; Hansen, M. R.; Pardi, A. *J. Am. Chem. Soc.* **2000**, *122*, 11561−11562.
(6) Bayer, P.; Varani, L.; Varani, G. *J. Biomol. NMR* **1999**, *14*, 149−155.
(7) Sibille, N.; Pardi, A.; Simorre, J. P.; Blackledge, M. *J. Am. Chem. Soc.* **2001**, *123*, 12135−12146.
(8) Stefl, R.; Wu, H. H.; Ravindranathan, S.; Sklenar, V.; Feigon, J. *Proc. Natl. Acad. Sci. U.S.A.* **2004**, *101*, 1177−1182.
(9) MacDonald, D.; Lu, P. *Curr. Opin. Struct. Biol.* **2002**, *12*, 337−343.
(10) Barbic, A.; Zimmer, D. P.; Crothers, D. M. *Proc. Natl. Acad. Sci. U.S.A.* **2003**, *100*, 2369−2373.
(11) Wu, Z. R.; Maderia, M.; Barchi, J. J.; Marquez, V. E.; Bax, A. *Proc. Natl. Acad. Sci. U.S.A.* **2005**, *102*, 24−28.
(12) Tjandra, N.; Bax, A. *Science* **1997**, *278*, 1111−1114.
(13) Hansen, M. R.; Mueller, L.; Pardi, A. *Nature Struct. Biol.* **1998**, *5*, 1065−1074.
(14) Clore, G. M.; Starich, M. R.; Gronenborn, A. M. *J. Am. Chem. Soc.* **1998**, *120*, 10571−10572.

of the intrinsic magnetic susceptibility anisotropy of the molecules themselves.[18−24]

To date, most measurements of RDCs have focused on one-bond $^{13}C-^{1}H$, $^{15}N-^{1}H$, $^{13}C-^{13}C$, and $^{13}C-^{15}N$ interactions, although two-bond $^{13}C-^{1}H$ and $^{15}N-^{1}H$ and longer-range $^{1}H-^{1}H$ and $^{1}H-^{31}P$ interactions also have proven useful, particularly in moderately sized oligonucleotides.[25−29] Incomplete averaging of the chemical shift anisotropy (CSA) upon alignment manifests itself in a change in the resonance position.[30,31] For a given nucleus, this change depends on the magnitude of the chemical shift tensor and its orientation relative to the alignment tensor. In proteins, the residual CSA effects (RCSAs) have proven particularly useful for backbone carbonyl sites, which have large and relatively uniform chemical shift tensors and for which the resonance positions can be determined at high accuracy, even in larger proteins.[32,33] In nucleic acids, RCSA measurement has primarily been restricted to backbone phosphate groups,[34] although recently such measurements were also used to define the CSA tensors of the ribose carbons in helical A-form RNA.[35] It is anticipated that for nucleic acid bases, where the $^{13}C$ CSA is rather large, RCSA effects will also be very useful. Base carbon RCSAs are of comparable magnitude to RDCs and can readily be measured at the required accuracy. In particular, because the CSA tensors have large magnitudes and are asymmetric for the protonated base carbons, RCSAs contain information on base orientation that complements the RDCs at the corresponding sites.[36]

Interpretation of base $^{13}C$ relaxation rates in terms of molecular motion can yield insights into important molecular recognition events. However, as also applies for RCSAs, quantitative analysis of the relaxation rates requires accurate knowledge of the $^{13}C$ CSA tensors, and a substantial range of CSA tensor magnitudes has been used previously, differing by as much as 30% for a given site. Mostly, but not universally, CSA values derived from NMR relaxation rates[37−40] have been higher than computed values.[41,42] In the model compound pyrimidine, relatively large $^{13}C$ CSA values, close to the highest values used in NMR relaxation studies, were observed by magic-angle-spinning (MAS) liquid crystal NMR.[31] Chemical shift tensors for the full set of polycrystalline deoxyribose mononucleosides have been reported relatively recently by Stueber and Grant.[43] The principal components were determined on slow magic-angle-spinning samples, using the solid-state FIREMAT NMR method, with tensor orientations obtained from embedded-ion-method (EIM) quantum chemical calculations. Considerable impact of the electrostatic crystal potentials was shown in this work, suggesting that some adjustment of the CSA values may be required for Watson−Crick base-paired oligonucleotides. The precision with which the CSA values can be extracted from the solid-state NMR spectra is good, although with the exception of the pyrimidine $C_5$ carbons, each protonated base carbon is adjacent to $^{14}N$, resulting in some interference by $^{14}N-^{13}C$ dipolar coupling. This is mainly observed as an asymmetric broadening of the otherwise sharp spinning sidebands, which are representative of the $^{13}C$ chemical shift tensor powder pattern. The quantum chemical calculations confirm that the tensors are symmetric with respect to the plane of the base, with the most-shielded component orthogonal to this plane, and indicate that the least-shielded component is oriented within about 30° of the C−H bond vector.

A recent $^{13}C$ relaxation study of an RNA oligomer by Schwalbe and Duchardt yielded systematically lower order parameters for purine $C_8-H$ compared to pyrimidine $C_6-H$ vectors when the Stueber and Grant CSA values were used, and these authors suggest that this paradoxical result could be explained by $C_6$ CSA values in helical RNA that are larger than those calculated or observed for mononucleosides.[44] A subsequent, very recent study of both the field dependence of $^{13}C$ transverse relaxation, $R_2$, as well as relaxation interference between the CSA and $^{13}C-^{1}H$ dipolar mechanisms, $\Gamma_{C,CH}$, in a B-form DNA oligomer also points to systematic differences between the literature CSA tensor values and those applicable in double-stranded Watson−Crick base-paired nucleotides.[45] However, this latter study could not uniquely determine the three unknown parameters, defining the magnitude and orientation of the traceless part of each chemical shift tensor, from the two experimental observables: $\Gamma_{C,CH}$ and field dependence of $R_2$. Here, we report a fully determined chemical shift tensor for each protonated base carbon on the basis of the small chemical shift changes that occur upon weak alignment, resulting from incomplete averaging of the CSA, complemented by relaxation measurements carried out on both a DNA and an RNA helix.

Schwalbe and Duchardt highlighted the need to ensure that the CSA values and dipolar interaction constants are properly scaled relative to one another. The dipolar interaction constant,


(15) Tycko, R.; Blanco, F. J.; Ishii, Y. *J. Am. Chem. Soc.* **2000**, *122*, 9340−9341.
(16) Sass, H.-J.; Musco, G.; Stahl, S. J.; Wingfield, P. T.; Grzesiek, S. *J. Biomol. NMR* **2000**, *18*, 303−309.
(17) Kim, I.; Lukavsky, P. J.; Puglisi, J. D. *J. Am. Chem. Soc.* **2002**, *124*, 9338−9339.
(18) Gayathri, C.; Bothnerby, A. A.; Vanzijl, P. C. M.; Maclean, C. *Chem. Phys. Lett.* **1982**, *87*, 192−196.
(19) Tolman, J. R.; Flanagan, J. M.; Kennedy, M. A.; Prestegard, J. H. *Proc. Natl. Acad. Sci. U.S.A.* **1995**, *92*, 9279−9283.
(20) Kung, H. C.; Wang, K. Y.; Goljer, I.; Bolton, P. H. *J. Magn. Reson. Ser. B* **1995**, *109*, 323−325.
(21) Bryce, D. L.; Boisbouvier, J.; Bax, A. *J. Am. Chem. Soc.* **2004**, *126*, 10820−10821.
(22) Al-Hashimi, H. M.; Tolman, J. R.; Majumdar, A.; Gorin, A.; Patel, D. J. *J. Am. Chem. Soc.* **2001**, *123*, 5806−5807.
(23) Van Buuren, B. N. M.; Schleucher, A.; Wittmann, V.; Griesinger, C.; Schwalbe, H.; Wijmenga, S. S. *Angew. Chem., Int. Engl. Ed.* **2004**, *43*, 187−192.
(24) Zhang, Q.; Throolin, R.; Pitt, S. W.; Serganov, A.; Al-Hashimi, H. M. *J. Am. Chem. Soc.* **2003**, *125*, 10530−10531.
(25) Yan, J. L.; Corpora, T.; Pradhan, P.; Bushweller, J. H. *J. Biomol. NMR* **2002**, *22*, 9−20.
(26) Zidek, L.; Wu, H. H.; Feigon, J.; Sklenar, V. *J. Biomol. NMR* **2001**, *21*, 153−160.
(27) Jaroniec, C. P.; Boisbouvier, J.; Tworowska, I.; Nikonowicz, E. P.; Bax, A. *J. Biomol. NMR* **2005**, *31*, 231−241.
(28) Boisbouvier, J.; Bryce, D. L.; O'Neil-Cabello, E.; Nikonowicz, E. P.; Bax, A. *J. Biomol. NMR* **2004**, *30*, 287−301.
(29) Wu, Z. R.; Tjandra, N.; Bax, A. *J. Biomol. NMR* **2001**, *19*, 367−370.
(30) Emsley, J. W.; Lindon, J. C. *NMR Spectroscopy using liquid crystal solvents*; Pergamon Press: Oxford, U.K., 1975.
(31) Fung, B. M.; Parhami, P. *J. Magn. Reson.* **1985**, *63*, 168−173.
(32) Lipsitz, R. S.; Tjandra, N. *J. Am. Chem. Soc.* **2001**, *123*, 11065−11066.
(33) Choy, W. Y.; Tollinger, M.; Mueller, G. A.; Kay, L. E. *J. Biomol. NMR* **2001**, *21*, 31−40.
(34) Wu, Z.; Delaglio, F.; Tjandra, N.; Zhurkin, V. B.; Bax, A. *J. Biomol. NMR* **2003**, *26*, 297−315.
(35) Bryce, D. L.; Grishaev, A.; Bax, A. *J. Am. Chem. Soc.* **2005**, *127*, 7387−7396.
(36) Hansen, A. L.; Al-Hashimi, H. M. *J. Magn. Reson.* **2006**, *179*, 299−307.
(37) Williamson, J. R.; Boxer, S. G. *Biochemistry* **1989**, *28*, 2819−2831.
(38) Hall, K. B.; Tang, C. *Biochemistry* **1998**, *37*, 9323−9332.
(39) Kojima, C.; Ono, A.; Kainosho, M.; James, T. L. *J. Magn. Reson.* **1998**, *135*, 310−333.
(40) Ravindranathan, S.; Kim, C. H.; Bodenhausen, G. *J. Biomol. NMR* **2005**, *33*, 163−174.
(41) Sitkoff, D.; Case, D. A. *Prog. Nucl. Magn. Reson. Spectrosc.* **1998**, *32*, 165−190.
(42) Fiala, R.; Jiang, F.; Sklenar, V. *J. Biomol. NMR* **1998**, *12*, 373−383.
(43) Stueber, D.; Grant, D. M. *J. Am. Chem. Soc.* **2002**, *124*, 10539−10551.
(44) Schwalbe, H.; Duchardt, E. *J. Biomol. NMR* **2005**, *32*, 295−308.
(45) Ying, J.; Grishaev, A.; Bax, A. *Magn. Reson. Chem.* **2006**, *44*, 302−310.

as observed in solid-state NMR, is affected by ultrafast internal motions, related to bond librations and vibrations.[46] These rapid motions result in an effective C−H bond length that is about 2−3% longer than that observed by neutron scattering.[46−49] Similarly, the observed span of the CS tensor already includes the effects of ultrafast motion, and the CSA values observed by solid-state NMR therefore represent vibrationally averaged values.

Our present study of CSA derives the degree of alignment from the observed RDCs. The characteristic alignment tensor is therefore inversely proportional to the dipolar interaction constant, which varies with $\langle r_{CH}^{-3} \rangle$. On the basis of both computational analysis[46] and the experimentally observed scaling factor for $C^{\alpha}-H^{\alpha}$ interactions in proteins relative to the less mobile peptide group $C^{\alpha}-C'$ and $C'-N$ interactions,[49] we use a uniform, effective C−H bond length of 1.104 Å for all protonated base carbons, instead of the standard 1.08 Å distance often used in aromatic systems.[50] All CSA values reported in the present study are scaled relative to this 1.104-Å value.

## Materials and Methods

**Sample Preparation.** Two samples of a uniformly $^{13}C$, $^{15}N$-enriched 24-nucleotide stem-loop RNA oligomer, derived from helix-35 of *E. coli* 23S ribosomal RNA and modified with pseudouridine ($\psi$) at the position corresponding to residue 746, were used. The nucleotide sequence, r(GGGCUAAUG$\psi$UGAAAAAUUAGCCC), for brevity is referred to as G1−C24 in this paper (instead of G737−C760). Special care was taken that, except for the presence or absence of 25 mg/mL of filamentous phage Pf1[13] purchased from Asla Biotech Ltd. (Riga, Latvia, http://www.asla-biotech.com/asla-phage.htm), the solution conditions of the two samples were as similar as possible.[27] Both samples were in thin-wall Shigemi microcells (300 $\mu$L), and each contained 1.5 mM helix-35$\psi$, 17 mM NaCl, 17 mM potassium phosphate, and 0.03 mM EDTA in 99% $D_2O$ at pH 6.8. The $^2H$ lock solvent quadrupole splitting observed for the Pf1 aligned sample was 28.3 Hz at 298 K. To obtain reliable anisotropic chemical shift measurements, both samples were dialyzed overnight against the same buffer, thereby further minimizing the effect of differential sample conditions on the chemical shifts.

Two natural abundance $^{13}C$ samples of 1.8 mM d(CGCGAATTCGCG)$_2$ (3.6 mM monomer) were prepared in $D_2O$, each in a 270 $\mu$L Shigemi microcell. One sample contained 18 mg/mL of Pf1, and the second sample was isotropic. Both samples were initially prepared to have approximately the same buffer conditions and subsequently dialyzed simultaneously overnight against a $D_2O$ buffer solution containing 50 mM KCl, 1 mM EDTA, 0.02% $NaN_3$, and 10 mM sodium phosphate buffer, pH 7.0 (apparent meter reading). The $^2H$ lock solvent quadrupole splitting observed for the Pf1-aligned sample was 20.8 Hz at 298 K.

**NMR Spectroscopy.** NMR spectra were recorded at 298 K on Bruker DRX800, DRX600, and DMX500 spectrometers, each equipped with a triple-resonance cryogenic probehead containing a *z* axis pulsed-field-gradient accessory. Longitudinal and transverse relaxation rates of the two $^{13}C-\{^1H\}$ doublet components were recorded for the base sites in d(CGCGAATTCGCG)$_2$ and processed in the same manner as described recently.[45] Results were averaged with those of these earlier experiments[45] to reduce random error. Relaxation rates in the uniformly $^{13}C/^{15}N$-enriched RNA sample were recorded with slightly modified sequences, which employed a nonselective 180° pulse immediately followed by a selective 180° pulse at the center of the $t_1$ evolution period to remove homonuclear $^{13}C-^{13}C$ couplings. Transverse relaxation rates were measured both in the Hahn-echo mode and in the spin-locked ($R_{1\rho}$) mode. Apparent spin-locked relaxation rates, $R_{1\rho,app}$, were converted to on-resonance $R_{1\rho}$ values in the regular manner, using $R_{1\rho,app} = \sin^2\zeta\, R_{1\rho} + \cos^2\zeta\, R_1$, with $\zeta$ being the angle between the effective RF field and the static magnetic field. Because $\zeta$ falls in the $90 \pm 15°$ range for all nuclei for which $R_{1\rho}$ was measured, the $\cos^2\zeta$ term is very small, and an approximate measurement of the longitudinal relaxation rate, $R_1$, suffices. Mostly, Hahn-echo and corrected $R_{1\rho}$ values were closely correlated. For adenine, however, the small chemical shift separation between the $^3J_{CC}$-coupled adenine $C_2$ and $C_5$ nuclei made it difficult to completely eliminate homonuclear Hartmann−Hahn contributions when measuring the $C_2$ $R_{1\rho}$ values in RNA, and therefore, these were not used. For thymidine $C_6$ carbons in the DNA dodecamer, the value measured for $R_{1\rho}$ of the downfield (TROSY) component of the $^{13}C$ doublet, $R_{1\rho}^{\beta}$ (where $\beta$ refers to the spin state of the attached $^1H$),[51] exhibits a small but systematic decrease of ca. 2 $s^{-1}$ relative to the $R_2^{\beta}$ value[51] measured by the Hahn-echo method. This decrease is attributed to the $^{13}C$ dephasing that occurs for this component under the influence of $^3J_{CH}$ couplings to the $T-C_5H_3$ protons during Hahn-echo delays for which $^3J_{CH}$ dephasing is not negligible, together with the relatively short $T_1$ of these methyl protons. Therefore, for $T-C_6$ only the $R_{1\rho}$ data were used for the analysis. $R_{1\rho}^{\alpha}$ and $R_{1\rho}^{\beta}$ values for $A-C_8$ and $G-C_8$, which resonate close to $T-C_6$, showed no systematic difference relative to the respective Hahn-echo $R_2^{\alpha}$ and $R_2^{\beta}$ values, and averaged values were used. $C-C_6$ resonances resonate further downfield, and their apparent $R_{1\rho}^{\alpha}$ and $R_{1\rho}^{\beta}$ values require a larger $R_1$ correction than their respective $R_2^{\alpha}$ and $R_2^{\beta}$ values.[51] Because the $R_1$ decay of individual $^{13}C_6$ doublet components is nonexponential and therefore less straightforward, the transverse relaxation analysis of $C-C_6$ was restricted to the Hahn-echo $R_2$ data. To avoid homonuclear $J_{CC}$ modulation of intensities after the Hahn-echo period for the uniformly $^{13}C$-enriched RNA sample, a band-selective REBURP-type 180° pulse[52] was used, covering bandwidths of 10, 10, and 3 ppm for $C_5$, $C_6/C_8$, and $C_2$ carbons, respectively. $^{13}C$ longitudinal relaxation times were measured using the pulse scheme of Farrow et al.,[53] again using a combination of nonselective and selective 180° pulses at the center of the $t_1$ evolution period for the RNA sample to remove homonuclear $^{13}C-^{13}C$ couplings. Relaxation of antiphase $C_zH_z$ terms was measured using the method of Wang et al.[54]

Changes in chemical shift between isotropic and aligned samples were measured by comparing chemical shifts in 2D gradient-enhanced $^1H-^{13}C$ HSQC spectra,[55] recorded again using a combination of a nonselective 180° pulse immediately followed by a selective 180° pulse at the center of the $t_1$ evolution period to remove homonuclear $^{13}C-^{13}C$ couplings. Because of the requirement to invert only the nuclei of interest by the selective 180° pulse, and not their $^{13}C$ coupling partners, three separate spectra were recorded for the adenine $C_2-H$ correlations, the $C_6-H$ and $C_8-H$ correlations, and the $C_5-H$ correlations in the uniformly $^{13}C$-enriched RNA sample, whereas for the natural abundance DNA sample the $C_2-H$, $C_6-H$ and $C_8-H$ correlations were detected simultaneously, and the considerably upfield-shifted $C_5-H$ correlations were measured separately. The effect of the $^2H$ residual quadrupolar lock signal splitting on the change in apparent chemical shift was accounted for by measuring the precise frequency of the residual HDO

(46) Case, D. A. *J. Biomol. NMR* **1999**, *15*, 95−102.
(47) Roberts, J. E.; Harbison, G. S.; Munowitz, M. G.; Herzfeld, J.; Griffin, R. G. *J. Am. Chem. Soc.* **1987**, *109*, 4163−4169.
(48) Hiyama, Y.; Niu, C. H.; Silverton, J. V.; Bavoso, A.; Torchia, D. A. *J. Am. Chem. Soc.* **1988**, *110*, 2378−2383.
(49) Ottiger, M.; Bax, A. *J. Am. Chem. Soc.* **1998**, *120*, 12334−12341.
(50) Allen, F. H.; Kennard, O.; Watson, D. G.; Brammer, L.; Orpen, A. G.; Taylor, R. *J. Chem. Soc., Perkin Trans. 2* **1987**, S1−S19.
(51) Igumenova, T. I.; Palmer, A. G. *J. Am. Chem. Soc.* **2006**, *128*, 8110−8111.
(52) Geen, H.; Freeman, R. *J. Magn. Reson.* **1991**, *93*, 93−141.
(53) Farrow, N. A.; Muhandiram, R.; Singer, A. U.; Pascal, S. M.; Kay, C. M.; Gish, G.; Shoelson, S. E.; Pawson, T.; Forman-Kay, J. D.; Kay, L. E. *Biochemistry* **1994**, *33*, 5984−6003.
(54) Wang, C. Y.; Rance, M.; Palmer, A. G. *J. Am. Chem. Soc.* **2003**, *125*, 8968−8969.
(55) Kay, L. E.; Keifer, P.; Saarinen, T. *J. Am. Chem. Soc.* **1992**, *114*, 10663−10665.

resonance for each sample and subtracting the difference frequency (in ppm) from the observed frequency difference between resonances in the aligned and isotropic samples. With this procedure, the average absolute difference in $^1$H frequency for the ribose $C_1'$ H protons in the aligned and isotropic samples was less than 1.6 ppb, in good agreement with the small CSA of aliphatic protons, and less than 4 ppb for the base protons.

Base RDCs were determined by measurement of the "half-splittings", $(^1D_{CH} + {}^1J_{CH})/2$, from the difference in $^{13}$C frequency between the $^{13}$C TROSY component and the corresponding $^1$H-decoupled HSQC frequency, recorded in interleaved spectra.[56] Although, by measuring effectively $^1D_{CH}/2$, the error in such a measurement is doubled when $^1D_{CH}$ is extracted, this method avoids the need to measure the precise $^{13}$C frequency of the very broad and weak, upfield anti-TROSY $^{13}$C doublet component. $^1D_{CH}$ values derived in this manner correlate very closely (Pearson's correlation coefficient, $R_P > 0.99$; root-mean-square difference (rmsd) < 1.2 Hz) with the values originally used for the structure determination of both the RNA helix[35] and the DNA dodecamer.[34] As expected, direct singular-value decomposition (SVD) fitting[57] of the RDCs to the previously determined structures yielded an alignment tensor very similar to the original one, after it was scaled by a constant factor equal to the ratio of the presently measured couplings to those used for the original structure calculations.

All spectra were processed and analyzed using NMRPipe.[58] The time-domain data were apodized in the indirect dimension by a 54°-shifted sine bell function and truncated at 176°; a 72°-shifted squared sine bell was used in the directly detected dimension. Time-domain data in the $^1$H and $^{13}$C dimensions were zero-filled to yield final digital resolutions of 3.9 and 2.4 Hz, respectively, and three-data-point parabolic interpolation was used for determining peak positions. At least two replicate measurements of all datasets were made over a period of 12 weeks to estimate the precision of the results and improve them by averaging. Averaged values were used for all analyses. The $^2$H lock splitting was monitored frequently and remained constant within 0.1 Hz over this period.

**Quantum Chemical Calculations.** Calculations of nuclear magnetic shielding tensors were carried out using Gaussian 03[59] running on computers of the High-Performance Computing Virtual Laboratory (HPCVL, University of Ottawa) and on the Biowulf cluster at the Division of Computer Research and Technology, at the National Institutes of Health. Calculations were performed on individual nucleotide fragments consisting of base, sugar, and phosphate moieties, as well as Watson−Crick base pairs where sugar moieties were replaced by methyl groups. The geometries were taken from the high-resolution X-ray structure of an A-form RNA helix (PDB entry 397D)[60] and the NMR structure of helix-35 RNA (PDB 2GBH)[61] which also contains an A-form helical segment. For DNA calculations, the NMR structure of the B-form DNA dodecamer d(CGCGAATTCGCG)$_2$ (PDB 1NAJ)[34] was used for individual nucleotides, and the 1ENN X-ray structure was used for the Me-A/Me-T basepair.[62]

Two sets of geometry optimizations and magnetic shielding tensor calculations were performed. One set of geometries was partially optimized at the restricted Hartree−Fock (RHF) level using the 6-311++G** basis set,[63,64] and calculations of the nuclear magnetic shielding tensors were then performed on the resulting geometries at the same level of theory. A second set of partially optimized geometries was generated using the B3LYP[65] hybrid functional and the 6-311++G** basis set; calculations of the nuclear magnetic shielding tensors were then performed on the resulting geometries at the same level of theory. The gauge-including atomic orbitals (GIAO) method[66,67] was used in all cases. The resulting symmetric parts of the magnetic shielding tensors were diagonalized to determine their principal components and orientations with respect to the molecular framework. Calculated magnetic shielding tensor eigenvalues were converted to the principal components of the traceless part of the chemical shift tensor ($\delta_{XX}$, $\delta_{YY}$, $\delta_{ZZ}$) according to $\delta_{ii} = \sigma_{iso} - \sigma_{ii}$, where $\sigma_{ZZ} \geq \sigma_{YY} \geq \sigma_{XX}$ and $\delta_{XX} \geq \delta_{YY} \geq \delta_{ZZ}$, and $\sigma_{iso} = (\sigma_{XX} + \sigma_{YY} + \sigma_{ZZ})/3$.

During the process of geometry optimization, base pairing was kept close to that observed crystallographically, by enforcing two interbase distances ($AN_6-TO_4$ and $AN_1-TN_3$), one dihedral angle ($AN_6-AN_1-TN_3-TO_4$), and two angular restraints ($AC_5-AN_1-TN_3$ and $TC_6-TN_3-AN_1$). Similarly, calculations on an A−U pair without the ribose moieties were also performed.

## Results

**Analysis of $^{13}$C Relaxation.** Interference between the $^{13}$C−{$^1$H} dipolar and the $^{13}$C CSA relaxation mechanisms can result in pronounced differences in the transverse relaxation rates of the two components of a $^{13}$C−{$^1$H} doublet.[68] This effect underlies the important TROSY-type NMR experiments, aimed at optimizing spectral resolution by selecting the slowest-relaxing components of the spectrum.[69,70] Quantitative measurement of the relaxation interference effect has been used to extract information on the CSA tensor for a variety of nuclei, including $^{15}$N, $^{13}C'$, and $^{13}C^{\alpha}$ sites in proteins,[71−74] and protonated base carbons in nucleic acids.[75] These latter measurements employed moderate levels of $^{13}$C enrichment, combined with isotope filtering to suppress signals from $^{13}$C nuclei with a direct $^{13}$C neighbor, thereby removing problems related to $^{13}$C−$^{13}$C $J$ couplings, as well as dipolar $^{13}$C−$^{13}$C contributions to the relaxation. Another study focused on purine $C_8$ and adenine $C_2$ sites, which lack directly bonded $^{13}$C nuclei.[40] In our present study, we measure both the field dependence of the transverse relaxation rate and the interference between the $^{13}$C−{$^1$H} dipolar and the $^{13}$C CSA relaxation mechanisms. Measurements carried out for the natural abundance $^{13}$C DNA sample, d(CGCGAATTCGCG)$_2$, largely duplicate results reported recently for a similar, slightly more concentrated sample.[45] The natural abundance $^{13}$C level removes the necessity to incorporate filtering elements in the pulse sequence and allows for very straightforward measurement using standard procedures. With the exception of $T-C_6$ (see Experimental Section), results were within the standard error of the earlier measurements, and the

(56) Kontaxis, G.; Clore, G. M.; Bax, A. *J. Magn. Reson.* **2000**, *143*, 184−196.
(57) Losonczi, J. A.; Andrec, M.; Fischer, M. W. F.; Prestegard, J. H. *J. Magn. Reson.* **1999**, *138*, 334−342.
(58) Delaglio, F.; Grzesiek, S.; Vuister, G. W.; Zhu, G.; Pfeifer, J.; Bax, A. *J. Biomol. NMR* **1995**, *6*, 277−293.
(59) Frisch, M. J. et al. *Gaussian 03*, revision C.02; Gaussian Inc.: Wallingford, CT, 2004.
(60) Ippolito, J. A.; Steitz, T. A. *Proc. Natl. Acad. Sci. U.S.A.* **1998**, *95*, 9819−9824.
(61) O'Neil-Cabello, E.; Bryce, D. L.; Nikonowicz, E. P.; Bax, A. *J. Am. Chem. Soc.* **2004**, *126*, 66−67.
(62) Soler-Lopez, M.; Malinina, L.; Subirana, J. A. *J. Biol. Chem.* **2000**, *275*, 23034−23044.
(63) McLean, A. D.; Chandler, G. S. *J. Chem. Phys.* **1980**, *72*, 5639−5648.
(64) Krishnan, R.; Binkley, J. S.; Seeger, R.; Pople, J. A. *J. Chem. Phys.* **1980**, *72*, 650−654.
(65) Becke, A. D. *J. Chem. Phys.* **1993**, *98*, 5648−5652.
(66) Ditchfield, R. *Mol. Phys.* **1974**, *27*, 789−807.
(67) Wolinski, K.; Hinton, J. F.; Pulay, P. *J. Am. Chem. Soc.* **1990**, *112*, 8251−8260.
(68) Goldman, M. *J. Magn. Reson.* **1984**, *60*, 437−452.
(69) Pervushin, K.; Riek, R.; Wider, G.; Wuthrich, K. *Proc. Natl. Acad. Sci. U.S.A.* **1997**, *94*, 12366−12371.
(70) Brutscher, B.; Boisbouvier, J.; Pardi, A.; Marion, D.; Simorre, J. P. *J. Am. Chem. Soc.* **1998**, *120*, 11845−11851.
(71) Tjandra, N.; Szabo, A.; Bax, A. *J. Am. Chem. Soc.* **1996**, *118*, 6986−6991.
(72) Tjandra, N.; Bax, A. *J. Am. Chem. Soc.* **1997**, *119*, 9576−9577.
(73) Tjandra, N.; Bax, A. *J. Am. Chem. Soc.* **1997**, *119*, 8076−8082.
(74) Fushman, D.; Tjandra, N.; Cowburn, D. *J. Am. Chem. Soc.* **1998**, *120*, 10947−10952.
(75) Boisbouvier, J.; Brutscher, B.; Simorre, J. P.; Marion, D. *J. Biomol. NMR* **1999**, *14*, 241−252.

averaged values are used for all further analyses (Supporting Information).

Uniform isotopic $^{13}C$ enrichment was needed for the measurements on RNA to achieve the required sensitivity. In our measurements, the effect of $^{13}C-^{13}C$ $^1J_{CC}$ modulation was removed using a band-selective (either $A-C_2$, $A-C_8/G-C_8$/$U-C_6/C-C_6$, or $U-C_5/C-C_5$) 180° pulse at the midpoint of the Hahn-echo transverse relaxation delay, instead of the regular nonselective 180° pulse. During both the DNA and the RNA transverse relaxation measurements, care was taken that the Hahn-echo transverse relaxation delay periods were integral multiples of $1/J_{CH}$, such that the transverse $^{13}C$ magnetization is an equally proportioned average over in-phase $C^+$ and antiphase $C^+H_z$ terms. The symbol $R_2$, used in this work, refers to this averaged relaxation rate, which carries averaged coefficients for the high-frequency spectral density components compared to those applicable for either the in-phase or antiphase $^{13}C$ magnetization.[74] Experimentally, the small values of the heteronuclear NOE ($\leq 1.3$)[44] indicate that these high-frequency contributions are negligible compared to $J(0)$.

In contrast, homonuclear $^1H-^1H$ dipolar relaxation, which contains a $J(0)$ spectral density term, considerably impacts the relaxation of $C^+H_z$. This effect was quantitatively accounted for by measurement of the difference between the longitudinal relaxation rates of the $C_z$ and $C_zH_z$ terms.[76] In addition, for the RNA sample, the spin−echo durations were selected such that they are approximately uniformly distributed over an integral multiple of the applicable $^1J_{CC}$ values. This makes the application of a first-order correction for the "passive spin lifetime effect" on the observed $R_2(^{13}C)$ possible. This lifetime effect refers to an increase in the apparent transverse $^{13}C$ relaxation rate that occurs when the $J$-coupled passive spin, $C^P$, changes its spin state because of an external relaxation source (either its CSA or dipolar interaction with a third spin), at a time when the $^{13}C$ magnetization of interest is antiphase with respect to this passive spin.[76] Approximate corrections to the measured $R_2(^{13}C)$ rates for both the TROSY and anti-TROSY components of the $^{13}C-\{^1H\}$ doublet are made according to

$$R_2'(^{13}C) = R_2(^{13}C) - [R_1(^{13}C^P) + R_1(^1H)]/2 \qquad (1)$$

For protonated carbons, $R_1(^{13}C^P)$ was derived from the initial slope of a nonselective inversion recovery experiment.[77] The longitudinal relaxation rate of the nonprotonated $C_4$ carbon in U and C nucleotides was approximated to be half that of the average rate observed for protonated carbons at 800 MHz $^1H$ frequency. Note that these lifetime effects impact the measured $^{13}C$ transverse relaxation rates by only a few percent. Therefore, modest errors in these corrections, resulting from approximations such as the $^{13}C$ recovery being exponential or from the uncertainty in the longitudinal relaxation rate of the nonprotonated carbons, have a negligible effect when analyzing the relaxation rates, which already have an experimental uncertainty of several percent. Below, for brevity and following commonly used nomenclature, the transverse relaxation rate corrected using eq 1 is simply referred to as $R_2$. Relaxation rates measured for the helical stem residues in the RNA oligomer are summarized in the Supporting Information.

Conformational exchange on a micro- to millisecond time scale can also contribute to transverse relaxation rates. The absence of measurable exchange contributions in the spectrum of the DNA oligomer was previously established by measuring the temperature dependence of the transverse relaxation rate of the TROSY component.[45] This slowly relaxing component is a particularly sensitive monitor of conformational exchange contributions to the transverse relaxation rate.[54] For the RNA sample, the presence of conformational exchange is indicated for nucleotides U8 and U18, which in addition to fast relaxation of the TROSY $^{13}C_6$ component also exhibit a strong temperature dependence of the relaxation rate, with a 50% faster transverse relaxation at 15 °C than at 25 °C (compared to 34 ± 3% for the remaining protonated base carbons, Supporting Information). Moreover, fast transverse relaxation of $^{13}C_1'$ results in weaker than average intensity for these nucleotides in the $^{13}C_1'-^1H_1'$ CT-HSQC spectra (data not shown). These nucleotides were therefore excluded from further relaxation analysis.

Transverse $^{13}C$ relaxation rates are dominated by $J(0)$ spectral density terms, and the same fractional increase by a factor 1.34 is observed for all RNA stem residues, except for U8, U18, and the terminal CG basepair, for both the TROSY and anti-TROSY components. Interestingly, this increase is slightly larger than the factor of 1.26 that would be expected on the basis of the change in $D_2O$ viscosity and the $1/kT$ dependence of the rotational diffusion alone. We speculate that the slightly larger than expected temperature dependence results from a stiffening of the loop region at lower temperature. Other indications for the increase in the effective length of the molecule at lower temperature are found in a 17% increase in alignment strength and a 27% decrease in alignment rhombicity when the temperature is lowered from 25 to 5 °C, pointing toward a more elongated shape.

All relaxation analyses use the standard equations, applicable for analysis of in-phase $^{13}C$ transverse relaxation rates and include all dipolar interactions to spins within a 3 Å radius and an anisotropic model for rotational diffusion.[78,79] Analysis of the relaxation rates is carried out as described previously for the DNA dodecamer using $^{13}C$ chemical shift tensors which are assumed to have one of their principal axes (which is shown to be the most shielded direction, $\delta_{ZZ}$) orthogonal to the plane of the base. When only the traceless part of the chemical shift tensor (i.e., $\delta_{XX} + \delta_{YY} + \delta_{ZZ} = 0$) is considered, this leaves three adjustable CSA parameters: its magnitude, $|\delta^M| = (\delta_x^2 + \delta_y^2 - \delta_x\delta_y)^{1/2}$, where $\delta_x = \delta_{XX} - \delta_{ZZ}$ and $\delta_y = \delta_{YY} - \delta_{ZZ}$; the asymmetry of the CSA, $\eta = (\delta_{YY} - \delta_{XX})/\delta_{ZZ}$; and the angle, $\theta$, between the $\delta_{XX}$ axis and the C−H bond. Note that $|\delta^M|$ can be rewritten as $|\delta^M| = (^3/_2)\delta_{ZZ}(1 + \eta^2/3)^{1/2}$. Initially, the analysis was performed under the assumption of a single chemical shift tensor for each given type of base carbon, and on the basis of prior work, $C_8$ carbons of A and G nucleotides were grouped together, as were $C_6$ of C, U, and T. Carbons $C_5$ of C and U were also grouped together, whereas the $C_2$ of A cannot be combined with other types, leaving a total of four chemical shift tensors to be determined. However, as will be discussed below, both the relaxation and RCSA data indicate a larger pyrimidine $C_6$ CSA in A-form RNA than in B-form DNA, necessitating their separate consideration during analysis. Similarly, in DNA,

(76) Peng, J. W.; Wagner, G. *J. Magn. Reson.* **1992**, *98*, 308−332.
(77) Boisbouvier, J.; Wu, Z. R.; Ono, A.; Kainosho, M.; Bax, A. *J. Biomol. NMR* **2003**, *27*, 133−142.
(78) Spiess, H. W. *NMR: Basic Princ. Prog.* **1978**, *15*, 55−214.
(79) Chang, S. L.; Tjandra, N. *J. Magn. Reson.* **2005**, *174*, 43−53.

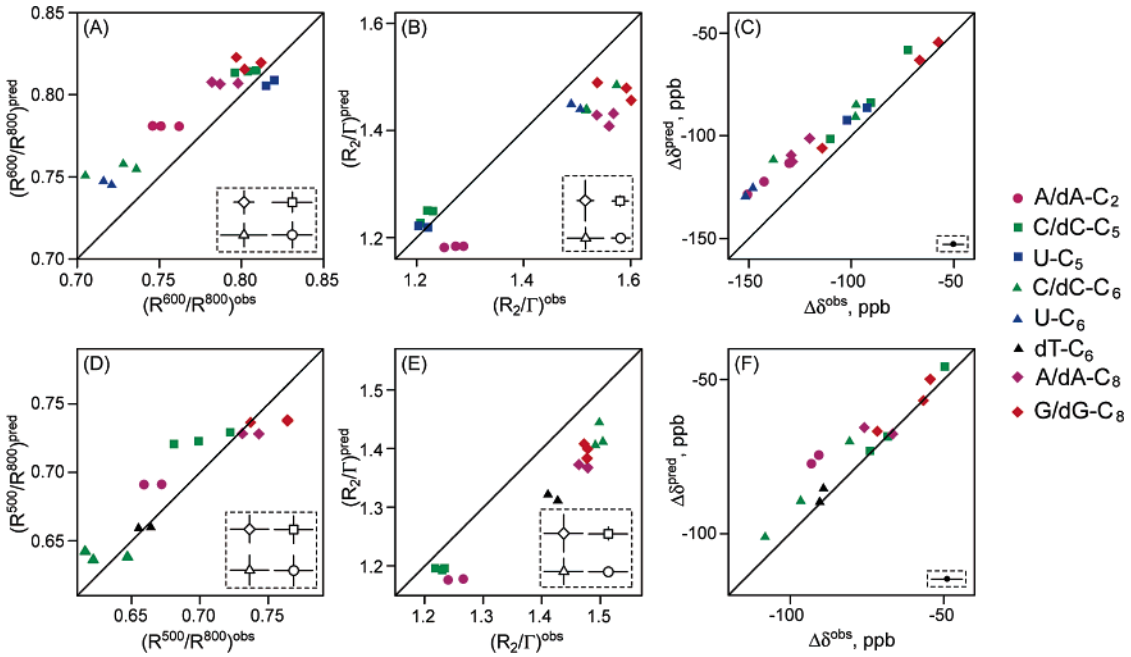


***Figure 1.*** Observed CSA-dependent parameters in (A−C) RNA and (D−F) DNA, versus values predicted on the basis of CSA values of Stueber and Grant.[43] (A, D) Field dependence of $(2R_2 - R_1)$, (B, E) ratio of $R_2$ and $\Gamma_{C,CH}$, (C, F) changes in chemical shift between aligned and isotropic phase. Error bars are indicated in the dashed insets. Errors in the observed parameters are derived from reproducibility of separate measurements. Errors in the predicted parameters reflect uncertainties in the diffusion anisotropy and the precision of the structures (1NAJ and 2GBH) used for calculating the predicted values.

the data indicate a smaller CSA for T−$C_6$ than for C−$C_6$, as well as differences between A−$C_8$ and G−$C_8$ tensors, and these bases are therefore considered separately too.

For both the DNA and the RNA oligomer, we find that fitting of the relaxation data does not yield any statistically significant improvement when using a fully asymmetric rotational diffusion tensor over an axially symmetric one, and all relaxation analyses therefore are carried out for an axially symmetric diffusion tensor. For the DNA oligomer, a rotational diffusion anisotropy of $D_\parallel/D_\perp = 2.1$ has previously been reported on the basis of deoxyribose $^{13}$C relaxation rates,[77] with the unique axis nearly parallel to the helical axis. Note that analysis of the base $^{13}$C relaxation rates alone provides insufficient information to uniquely establish the diffusion anisotropy because all base C−H vectors are roughly orthogonal to the helix axis. In contrast to the DNA oligomer, spectra for the RNA molecule exhibit extensive overlap of resonances in the ribose region, thereby prohibiting $^{13}$C relaxation measurements with standard 2D methods and accurate relaxation rates could only be measured for the well-dispersed base $^{13}$C−$^{1}$H correlations. Therefore, diffusion anisotropy of the RNA oligomer is treated as a variable in the fit, when simultaneously analyzing chemical shift changes resulting from alignment, $\Delta\delta$, and relaxation rates (vide infra).

**Field Dependence of $^{13}$C Transverse Relaxation.** As previously discussed by Fushman et al., the combination of relaxation times, $2R_2 - R_1$, is dominated by $J(0)$ spectral density terms and therefore is particularly well suited for determination of the magnitude of the CSA tensor, $|\delta^M|$.[80] Figure 1A plots the observed ratios of $(2R_2 - R_1)^{600MHz}/(2R_2 - R_1)^{800MHz}$ for the RNA sample versus the ratios computed on the basis of Stueber-and-Grant CSA values.[43] Figure 1D shows analogous ratios, $(2R_2 - R_1)^{500MHz}/(2R_2 - R_1)^{800MHz}$, for the DNA sample. The vertical error bars for the computed ratios correspond to the range of values computed for diffusion anisotropies, $D_\parallel/D_\perp$, ranging from 1.7 to 2.5 for DNA and from 1.6 to 2.4 for RNA. Increased errors for the $C_6$ and $C_8$ carbons reflect the fact that their CSA tensors have the largest $\theta$ angles, causing them to be more sensitive to variations in $D_\parallel/D_\perp$. Error bars for the measured values are based on reproducibility of the measurements.

As can be seen from the figure, in particular for the RNA sample, most of the observed ratios are smaller than predicted, which suggests a CSA magnitude that is higher than seen in isolated DNA mononucleosides by solid-state NMR. It is interesting to note that in both the RNA and DNA samples, experimental ratios for A−$C_8$ fall below those of G−$C_8$, in agreement with the predictions from solid-state data.[43] Larger ratios are observed for both DNA T−$C_6$ carbons than for the three C−$C_6$ nuclei (Figure 1D), also in good agreement with the solid-state data.

**Interference between CSA and $^{13}$C−$^{1}$H Dipolar Mechanisms.** As pointed out by Fushman and Cowburn,[81] under isotropic tumbling and in the slow tumbling limit, the ratio between the $^{13}$C transverse relaxation rate and the relaxation interference rate, to a good approximation, is given by

$$R_2/\Gamma_{C,CH} = [9\xi^2_{DD} + 4\gamma_C{}^2 B_0{}^2 |\delta^M|^2]/(12\xi_{DD}\gamma_C B_0\delta_p) \quad (2)$$

which is independent of the rotational correlation time. In this equation, the magnitude of the dipolar interaction constant, $\xi_{DD}$, is given by $\xi_{DD} = (\mu_0/4\pi)(h/2\pi)\gamma_C\gamma_H\langle r_{CH}{}^{-3}\rangle$, where $\gamma_X$ is the magnetogyric ratio of nucleus X, $B_0$ is the strength of the magnetic field, and $\delta_p$ is given by $\delta_p = P_2(\cos\theta^{xd})\delta_x + P_2(\cos\theta^{yd})\delta_y$, where $P_2(x) = (3x^2 - 1)/2$, $\theta^{xd}$ and $\theta^{yd}$ are the angles between the dipolar vector and the principal $x$ and $y$ axis of the

(80) Fushman, D.; Tjandra, N.; Cowburn, D. *J. Am. Chem. Soc.* **1999**, *121*, 8577−8582.

(81) Fushman, D.; Cowburn, D. *J. Am. Chem. Soc.* **1998**, *120*, 7109−7110.

CSA tensor (corresponding to principal components $\delta_{XX}$ and $\delta_{YY}$, respectively), and $\delta_x = \delta_{XX} - \delta_{ZZ}$ and $\delta_y = \delta_{YY} - \delta_{ZZ}$. Under anisotropic rotational diffusion, eq 2 is no longer valid, but the $R_2/\Gamma_{C,CH}$ ratio remains much less sensitive to both global tumbling and internal dynamics than either $R_2$ or $\Gamma_{C,CH}$. We therefore numerically evaluate the $R_2/\Gamma_{C,CH}$ ratio rather than $\Gamma_{C,CH}$.

The value of $R_2$ under fully anisotropic diffusion in the presence of dipolar and CSA interactions is calculated using the equations of Spiess.[78,79] The interference term, $\Gamma_{C,CH}$, is derived using the same equations, by calculating the difference for relaxation under two "pseudo-CSA" tensors that correspond to the sum and the difference of the dipolar and the CSA tensors.[45]

Figures 1B and 1E compare the observed $R_2/\Gamma_{C,CH}$ ratios with values calculated when using the CSA tensors of Stueber and Grant for the RNA and DNA oligomers. Agreement between the observed and calculated ratios is very good for $C_5$. Small, systematic differences are observed for the other types of carbons, with the observed $R_2/\Gamma_{C,CH}$ ratio for $C_2$ and $C_8$ carbons consistently being higher than computed, indicative of a somewhat smaller than anticipated relaxation interference term.

**Chemical Shift Changes upon Alignment.** The residual difference in chemical shift (RCSA) between weakly aligned ($\delta_{aniso}$) and isotropic ($\delta_{iso}$) samples is computed as[82]

$$\Delta\delta = \delta_{aniso} - \delta_{iso} = \sum_{i=X,Y,Z}\sum_{j=X,Y,Z} A_{jj}\cos^2(\theta_{ij})\delta_{ii} \qquad (3)$$

where $A_{jj}$ are the principal components of the molecular alignment tensor, $\delta_{ii}$ are the principal components of the CSA tensor, and $\theta_{ij}$ is the angle between principal axis, $j$, of the alignment tensor and principal axis, $i$, of the CSA tensor.

On the basis of the CSA magnitudes for base carbons, as determined by solid-state NMR,[43] chemical shift changes at 201 MHz $^{13}C$ frequency, resulting from weak alignment, span a range similar to residual $^1D_{CH}$ couplings. Indeed, considerable chemical shift changes are observed both for the DNA and the RNA oligomers (Figure 2). All observed chemical shift changes are in the upfield direction. This results from the fact that the most-shielded tensor component is orthogonal to the base plane for all four types of carbons studied, and in the oligomers used in this study, all base planes are oriented approximately orthogonal to the $z$ axis of the alignment tensor.

Previous measurements of the $^1D_{CH}$, $^1D_{CC,}$ $^1D_{CN}$, and $^2D_{CH}$ couplings for the RNA oligomer were highly self-consistent and yielded predicted $^1D_{CH}$ values that exhibit a rmsd of 1 Hz relative to measured base $^1D_{CH}$ values.[28] This 1 Hz rmsd results in part from measurement error in $^1D_{CH}$, but it is also affected by random uncertainty in the atomic coordinates, often referred to as structural noise,[83] which causes errors in the predicted couplings. Both the RCSA measurement error and the error in its predicted value resulting from structural noise are comparable to those for $^1D_{CH}$. Therefore, under the assumption of a uniform CSA tensor for all carbons of a given type, the lower limit for the rmsd of the difference between $\Delta\delta_i^{obs}$ and $\Delta\delta_i^{pred}$ is expected to be $X \approx 5$ ppb at 201 MHz. Therefore, an error function may be defined as

$$E^{\Delta\delta}(|\delta^M|,\eta,\theta) = (1/N)\sum_i\{[\Delta\delta_i^{obs} - \Delta\delta_i^{pred}]^2/X^2\} \qquad (4)$$

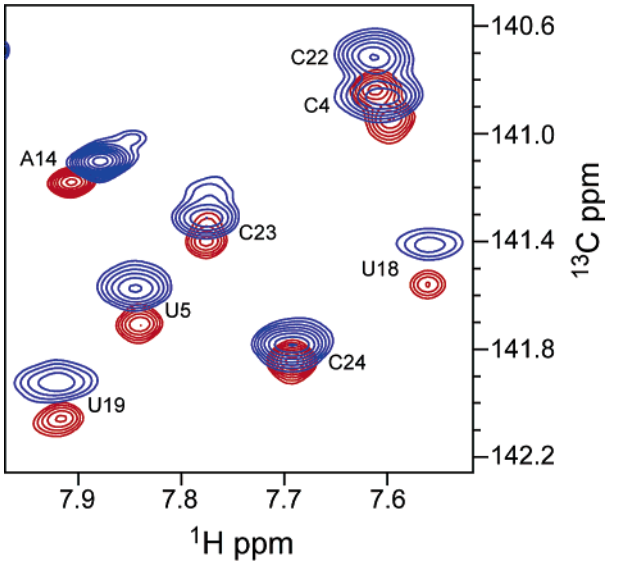


***Figure 2.*** Overlay of small regions of the 800 MHz homonuclear $^{13}C$-decoupled $^1H-^{13}C$ HSQC spectra spectra displaying $C_6-H_6$ correlations in helix-35 RNA: (red) isotropic phase and (blue) in Pf1 medium. The upfield change in $^1H$ chemical shift for A14$-H_8$ reflects a small change in the average structure for the flexible loop of helix-35 between isotropic and aligned media.

where $\theta$ is the angle (<90°) between the least shielded ($x$) axis of the CSA tensor and the C−H vector, with a positive sign of $\theta$ for rotations about the base plane normal in the direction that increases the angle between the $x$ axis and both the $C_8-H_8$ and the $C_8-N_9$ vectors in A/G, the $C_2-H_2$ and $C_2-N_1$ vectors in A, the $C_6-H_6$ and $C_6-N_1$ vectors in U/C, and the $C_5-H_5$ and $C_5-C_6$ vectors in U/C (Figure 3).

**Extracting CSA Tensors from Experimental Data.** The aim of our analysis is to find the $^{13}C$ CSA tensors that best agree with both the experimental RCSA and $^{13}C$ relaxation data. The latter include both the field dependence of $2R_2 - R_1$ and the $^{13}C$ relaxation interference data. This is accomplished by searching for the CSA tensor that minimizes the total error function

$$E^t(|\delta^M|,\eta,\theta) = 1/(3N)\{\sum_i\{[\Delta\delta_i^{obs} - \Delta\delta_i^{pred}]^2/X^2 + (FD_i^{obs} - FD_i^{pred})^2/Y^2 + (CC_i^{obs} - CC_i^{pred})^2/Z^2\}\} \qquad (5)$$

where $FD_i$ refers to the field dependence ratio, $(2R_2 - R_1)^{500MHz}/(2R_2 - R_1)^{800MHz}$ for the DNA oligomer and $(2R_2 - R_1)^{600MHz}/(2R_2 - R_1)^{800MHz}$ for the RNA. $CC_i$ refers to the cross correlation ratio $R_2/\Gamma_{C,CH}$ of carbon $i$. In addition to the random measurement error, $X$, $Y$, and $Z$ also include the effects that the approximation of identical CSA tensors for all carbons of a given type, regardless of their location within the molecule, is not strictly valid, as well as effects from uncertainty in the experimentally determined structures. Their values are selected on the basis of reproducibility of the $\Delta\delta_i$ measurement and the spread in the observed $FD_i$ and $CC_i$ ratios within the DNA and RNA molecules, yielding $X = 5$ ppb, $Y = 0.006-0.014$, and $Z = 0.015-0.034$, depending on the carbon and nucleotide types.

Inspection of Figure 1C indicates that the measured $\Delta\delta$ values in the RNA oligomer are generally larger than anticipated on the basis of the solid-state NMR-derived CSA tensors for

(82) Cornilescu, G.; Bax, A. *J. Am. Chem. Soc.* **2000**, *122*, 10143−10154.
(83) Zweckstetter, M.; Bax, A. *J. Biomol. NMR* **2002**, *23*, 127−137.

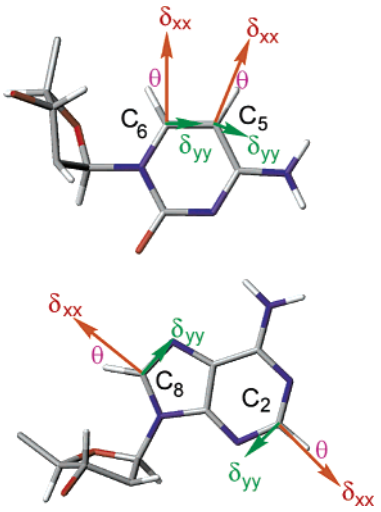


***Figure 3.*** Definition of the angle $\theta$ between the least shielded component of the CSA tensor and the C−H vector, for a cytosine and adenosine nucleotide. In the figure, depictions of $\theta$ correspond to positive values for $C_2$, $C_6$, and $C_8$ and to a negative value for $C_5$. The $\delta_{ZZ}$ axis is oriented orthogonal to the base plane.

deoxyribose nucleosides. For the DNA oligomer, this difference generally is much less pronounced, in particular for $C_6$. Similarly, the field dependence of the $C_6$ transverse relaxation rate is stronger than expected for RNA (Figure 1A) but nearly on target for DNA (Figure 1D), forcing us to analyze separately the results for $C_6$ in DNA and RNA. Systematic differences between DNA and RNA for the other types of carbons are considerably smaller, and the distinction between DNA and RNA resulted in no statistically significant differences when analyzed separately. Figures 1D and 1E indicate that the observed rates and $R_2/\Gamma$ ratios for the T−$C_6$ carbons deviate considerably from those of C−$C_6$, an observation supported by the previous data of Stueber and Grant, [43] and therefore requiring T−$C_6$ and C−$C_6$ in DNA to be treated separately.

Since both $\Delta\delta$ and the field dependence of relaxation rates are strongly affected by the magnitude of the CSA tensor, but only the field dependence is affected by the anisotropy of rotational diffusion, the $D_\parallel/D_\perp$ ratio for the RNA oligomer is obtained from a systematic search for the ratio that minimizes the residual $\chi^2$ when fitting the relaxation data and anisotropic shifts simultaneously, for all four carbon types. This analysis yields a diffusion anisotropy of $D_\parallel/D_\perp = 2.0 \pm 0.4$ (Supporting Information). Grid searches for the orientation of the $z$ axis of the diffusion tensor, performed separately for the four carbon types in the RNA, did not show a statistically significant deviation from the initial choice, where the $D_\parallel$ axis was assumed parallel to the $z$ axis of the molecular alignment tensor in Pf1 liquid crystalline medium (data not shown). This result agrees with previous analyses, which indicate that for steric or repulsive electrostatic interactions (negatively charged oligonucleotide in negative Pf1), the alignment tensor mirrors molecular shape[84] and therefore is similar in orientation to the rotational diffusion tensor.[85] The anisotropy, $D_\parallel/D_\perp = 2.0$, for the RNA oligomer is close to the ratio of 2.1 observed for the homodimeric, palindromic DNA dodecamer.[77] This similar degree of anisotropy is consistent with the notion that even while the loop region in the 24-nucleotide RNA oligomer is subject to increased internal dynamics, on average, the bases in this region remain in a stacked configuration, with their planes orthogonal to the axis of the helical stem region.[61]

Contour plots of orthogonal cross sections of $E^t(|\delta^M|,\eta,\theta)$ for each of the six carbon types indicate that the values of $|\delta^M|$, $\eta$, and $\theta$ compatible with the measured data span a considerable range and are highly correlated (Supporting Information). For example, for $C_8$, the optimal value of $\eta$ is strongly correlated with the value for $\theta$, complicating evaluation of the uncertainty in the extracted CSA parameters. Moreover, even while the experimentally observed parameters, $\Delta\delta_i^{obs}$, $FD_i^{obs}$, and $CC_i^{obs}$, can be fit very well when tensor parameters are optimized, only a modest number (as low as six, for the T−$C_6$ CSA) of experimental measurements are available to define the three CSA parameters. We address this issue by two separate methods: complete cross validation and Monte Carlo methods for estimating the effect of random error.

In the Monte Carlo approach, random Gaussian-distributed noise with a rms value equal to the error values $X$, $Y$, and $Z$ is added to each of the measured values, $\Delta\delta_i^{obs}$, $FD_i^{obs}$, and $CC_i^{obs}$, and the search for $|\delta^M|$, $\eta$, and $\theta$ values that minimize $E^t(|\delta^M|,\eta,\theta)$ is repeated 1000 times, using different sets of random noise. The results of this procedure are summarized in Figure 4, with the average and standard deviations in each of the three parameters listed in Table 1. For the DNA dC−$C_6$, Figure 4 shows that the angle, $\theta$, and asymmetry, $\eta$, cannot be determined independently. For the three dC−$C_6$ nuclei, the degenerate set of $(\theta,\eta)$ solutions available from the relaxation data cannot be resolved within experimental noise by adding the $\Delta\delta$ information (Figure 4, right column). However, when $\theta$ is restricted to an angle of 28° (selected on the basis of the RNA C−$C_6$ results and the quantum calculations), an $\eta$ value is obtained close to those obtained computationally and by Stueber and Grant.

In the jack-knife cross validation approach, a given triplet of experimentally observed $\Delta\delta_i^{obs}$, $FD_i^{obs}$, and $CC_i^{obs}$ values is omitted when using eq 5 to search for the CSA values that best fit the values for the remaining residues, while using the same standard errors for $X$, $Y$, and $Z$ as used above. The values of the omitted data points are then predicted using the resulting CS tensor, and the procedure is repeated for each nucleotide in the DNA and RNA oligomers, with results displayed in Figure 5. The statistics of the jack-knife cross-validation are listed in the Supporting Information.

**CSA Tensors from Quantum Chemical Calculations.** Geometries for isolated nucleotides were extracted from the NMR structure of the Dickerson dodecamer, from the helical segment of the NMR structure of ribosomal RNA helix-35, and from the X-ray structure of an A-form RNA helix. The models included the bases themselves, ribose sugar moieties, and phosphate groups. Prior to magnetic shielding calculations, geometries were partially optimized at either the B3LYP/6-311++G** or RHF/6-311++G** level of theory, while restraining the sugar pucker, the glycosidic torsion angle, $\chi$, and the $C_6$−$C_5'$ distance at the experimental values (see Experimental Section). Several of the calculations were carried out for a 1.2 Å RNA X-ray structure (PDB entry 466D),[86] after we

(84) Zweckstetter, M.; Hummer, G.; Bax, A. *Biophys. J.* **2004**, *86*, 3444−3460.
(85) de Alba, E.; Tjandra, N. *J. Magn. Reson.* **2000**, *144*, 367−371.
(86) Mueller, U.; Muller, Y. A.; Herbst-Irmer, R.; Sprinzl, M.; Heinemann, U. *Acta Crystallogr. D* **1999**, *55*, 1405−1413.

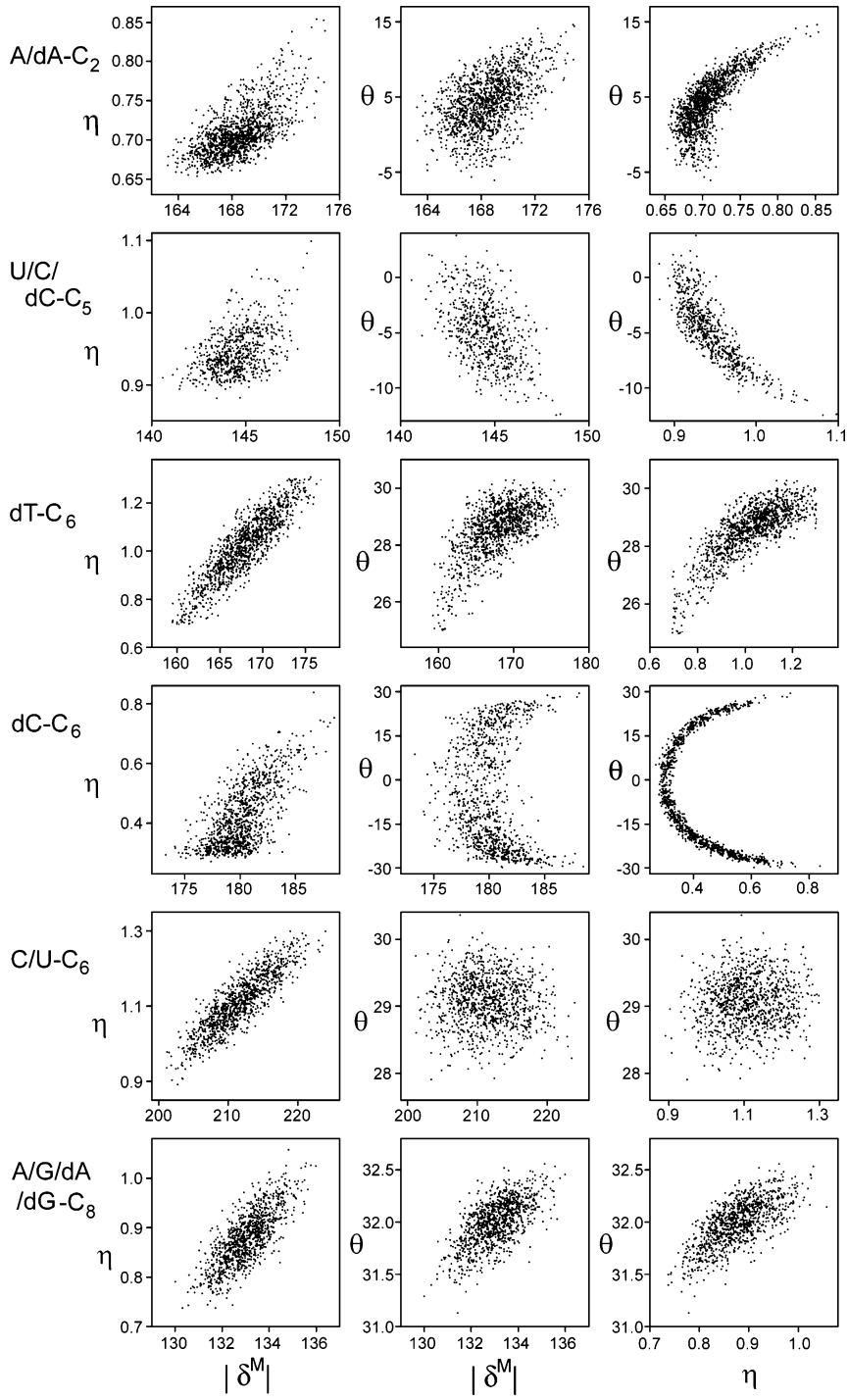


***Figure 4.*** Projections of best-fitted results onto two-dimensional planes of the three-dimensional parameter space ($|\delta^M|$, $\theta$, $\eta$) when 1000 best fits are carried out with random Gaussian noise added to the experimental data, with amplitudes of 5 ppb for $\Delta\delta$; 0.017 (A−$C_2$), 0.033 (dA−$C_2$), 0.015 (C−$C_5$), 0.033 (dC−$C_5$), 0.033 (dT−$C_6$), 0.033 (dC−$C_6$), 0.034 (U/C−$C_6$), 0.015 (A/G−$C_8$), and 0.033 (dA/dG−$C_8$) for the $R_2/\Gamma$ ratio, assuming identical CSA values for A−$C_8$ and G−$C_8$ carbons. Added random errors for the field-dependence ratio of $2R_2 - R_1$ were 0.012 (A−$C_2$), 0.014 (dA-$C_2$), 0.012 (C−$C_5$), 0.014 (dC−$C_5$), 0.014 (dT-$C_6$), 0.014 (dC−$C_6$), 0.014 (U/C−$C_6$), 0.006 (A/G−$C_8$) and 0.014 (dA/dG-$C_8$).

found that in the NMR structure of helix-35 the pyrimidine $C_6$H−O5′ distances are systematically 0.1−0.3 Å longer than in the highest resolution X-ray structures. Inspection of the NMR structure indicates that the $C_6$H−O5′ distances fall slightly below the sum of the $C_6$H and O5′ van der Waals radii, causing the empirical van der Waals term to become active and restrain their internuclear separation at values slightly larger than observed in high-resolution X-ray structures. Quantum calculations carried out to optimize the geometry of mononucleotides without the $C_6$−$C_5$′ distance restraint also resulted in a shortening of the $C_6$H−O5′ distance, but these geometry-optimized structures were not used for chemical shift calculations as it remained unclear to what extent the absence of water molecules in the geometry optimization affected the results. For NMR structures of the DNA oligomer, the $C_6$H−O5′ distance exceeds the limit where van der Waals radii start exerting an artificial force, and no systematic difference in $C_6$−$C_5$′ distance relative to DNA X-ray structures is found.

***Table 1.*** Carbon CSA Parameters Obtained from Relaxation and $\Delta\delta$ Measurements[a]

| atom | $\delta_{XX}$ (ppm) | $\delta_{YY}$ (ppm) | $\delta_{ZZ}$ (ppm) | $\theta$[b] (deg) | $\theta^{SG}$[c] (deg) | $\lvert\delta^{M}\rvert$ (ppm) | $\lvert\delta^{M}\rvert^{SG}$[c] (ppm) | $\eta$ | $\eta^{SG}$[c] |
|---|---|---|---|---|---|---|---|---|---|
| A/dA−$C_2$ | 89 ± 2 | 15 ± 2 | −104 ± 1 | 4 ± 4 | 3 | 168 ± 2 | 150 | 0.70 ± 0.03 | 0.92 |
| C/U/dC/dU−$C_5$ | 82 ± 1 | 2 ± 1 | −85 ± 1 | −5 ± 3 | 11 | 144 ± 1 | 138 | 0.95 ± 0.03 | 1.03 |
| dC−$C_6$ | 96 ± 2 | 19 ± 2 | −115 ± 1 | 28[d] | 29 | 186 ± 3 | 179 | 0.67 ± 0.03 | 0.83 |
| dT−$C_6$ | 97 ± 5 | −1 ± 6 | −96 ± 2 | 29 ± 1 | 30 | 168 ± 3 | 170 | 1.02 ± 0.13 | 1.17 |
| C/U−$C_6$ | 125 ± 4[e] | −7 ± 4[e] | −119 ± 1[e] | 29 ± 1 | *f* | 212 ± 4[e] | *f* | 1.11 ± 0.07[e] | *f* |
| G/dG−$C_8$[g] | 74 ± 2 | 5 ± 2 | −79 ± 1 | 32 ± 1 | 28 | 133 ± 1 | 126<br>134[h] | 0.88 ± 0.05 | 0.92<br>1.08[h] |
| A/dA−$C_8$[g] | 80 ± 2 | 5 ± 2 | −85 ± 1 | 32 ± 1 | 27 | 144 ± 1 | 134 | 0.88 ± 0.05 | 1.04 |

[a] Averages and uncertainties are determined as means and standard deviations of the best-fitted values within a set of 1000 Monte Carlo calculations, where random noise corresponding to the experimental rms uncertainties was added to all experimental values of $\Delta\delta$, FD, and CC. Because the effect of added noise on the best-fitted parameters is not symmetric, small differences occur between the averaged values listed in the table and those from a fit without added noise (Supporting Information). All fits are based on the absence of an $R_{ex}$ contribution to measured $R_2$ values, even though a small $R_{ex}$ value of up to 1 Hz cannot be excluded. Supporting Information Table 9 lists values extracted for the worst-case scenario, where all DNA and RNA $^{13}C$ $R_2$ values at 18.8 T simultaneously have a 1 Hz $R_{ex}$ contribution. Reported errors do not include the effect of uncertainty in diffusion anisotropy, $D_{\parallel}/D_{\perp}$. Values extracted when $D_{\parallel}/D_{\perp}$ is varied over its allowed range are reported in Supporting Information Table 10. [b] The angle $\theta$ is that between the $\delta_{XX}$ axis and C−H bond, which is assumed to coincide with the bisector of the heavy atom angle, with the sign of $\theta$ defined below eq 4. [c] Stueber-and-Grant CSA values.[43] [d] Angle could not be determined from the experimental data, and entries in this row correspond to values obtained when $\theta$ is kept fixed at 28°. [e] Considering the large value of $|\delta^{M}|$, relative to that expected on the basis of previous DNA measurements as well as the more moderate difference between computational results for DNA and RNA, we suggest that for future use the smallest CSA within our uncertainty range ($|\delta^{M}| = 208$ ppm, $\delta_{XX} = 121$ ppm, $\delta_{YY} = -3$ ppm, $\delta_{ZZ} = -118$ ppm, $\eta = 1.04$, and $\theta = 29°$) is preferred over that at the center of the allowed range. [f] Data not available. [g] The results for A and G were obtained via a joint fit with the difference between their $|\delta^{M}|$ best fitted to 11 ppm. [h] Data reported for two different molecules in the asymmetric unit.[43]

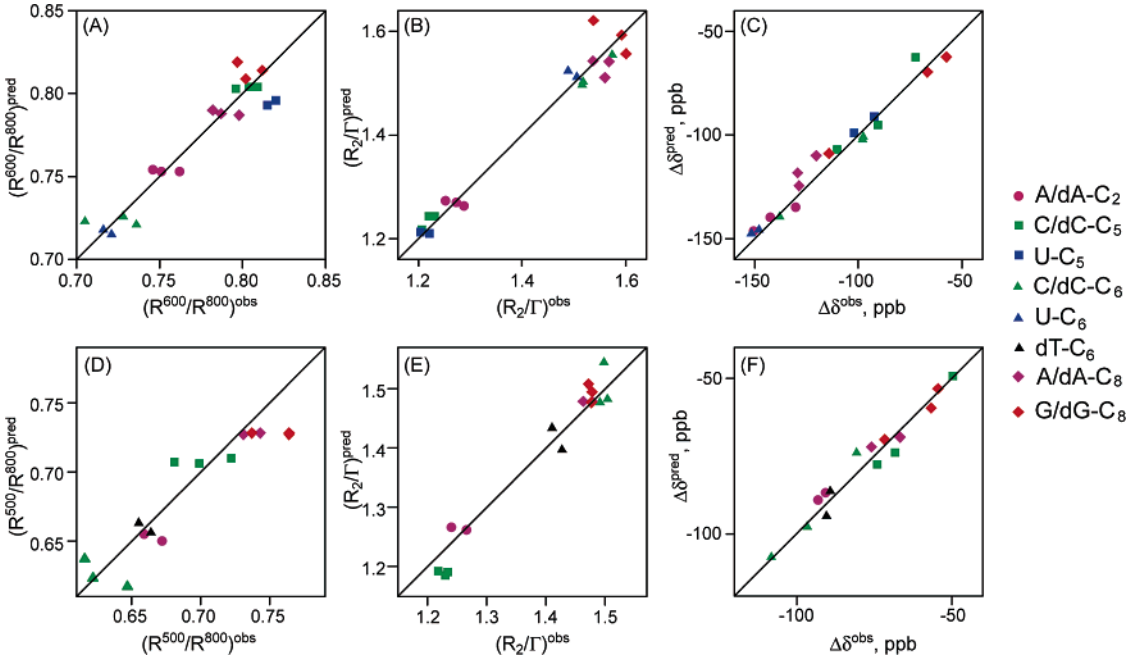


***Figure 5.*** Cross-validated predictions of CSA-related parameters versus observed values. The predicted values were obtained on the basis of CSA parameters resulting from a best-fit using the subset of bases from which the predicted nucleotide is excluded. (A−C) RNA bases and (D−F) DNA bases. (A, D) The ratio of $2R_2 - R_1$ at low (500 or 600 MHz) and high (800 MHz) field, (B, E) the $R_2/\Gamma$ ratio, and (C,F) $\Delta\delta$.

In the NMR structures, the precise relative positions of Watson−Crick bases are dominated by database-derived artificial restraints; therefore, the computed effect of base pairing on the A−$C_2$ chemical shift tensor was evaluated for basepair geometries extracted from high resolution RNA and DNA structures, followed by restrained geometry optimization (see Experimental Section). Convergence of the geometry optimization with the 6-311++G** basis set was only obtained when the structures were simplified by substituting a methyl group for the (deoxy)ribose moieties, and shielding calculations were carried out for these methyl-substituted A/U and A/T basepairs in the presence and absence of Watson−Crick base pairing.

For all base carbons, a significant increase in the magnitude of the CSA is observed when the RHF/6-311++G** method is used, compared to the B3LYP/6-311++G** method. This finding is in agreement with observations by Sitkoff and Case.[41] To gauge the effect of the basis set on calculated chemical shift tensors, B3LYP calculations with the 6-31G*, 6-311+G*, and 6-311++G** basis sets were carried out on a cytidine nucleotide. Remarkably, we find a rather large increase in the magnitude of the shielding anisotropy when diffuse and polarization functions are included on all heavy atoms, as well as hydrogens. Because the computations with the largest basis set exhibit best agreement with the experimental data of Stueber and Grant, as well as our own results, all computational results discussed in the text correspond to the B3LYP/6-311++G** level of theory. However, the substantial differences between restricted Hartree−Fock (Supporting Information) and B3LYP computational results (Table 2) highlight the uncertainty which remains when attempting to interpret the theoretical results in the absence of experimental data.

***Table 2.*** Nucleotide Base Carbon Chemical Shift Tensors as Determined by Quantum Chemical Calculations[a]

| nucleotide | residue atom | $\delta_{XX}$[b] (ppm) | $\delta_{YY}$ (ppm) | $\delta_{ZZ}$ (ppm) | $\theta$[c] (deg) | $\lvert\delta^M\rvert$ (ppm) | $\eta$ |
|---|---|---|---|---|---|---|---|
| dC[d] | C3−$C_6$ | 105.5 | 20.0 | −125.6 | 23.6 | 202.4 | 0.68 |
| dT[d] | T20-$C_6$ | 106.4 | −2.6 | −103.8 | 23.8 | 182.1 | 1.05 |
| A[e] | A7−$C_8$ | 77.0 | 6.5 | −83.5 | 28.5 | 139.3 | 0.85 |
| G[e] | G21−$C_8$ | 79.4 | −1.5 | −77.8 | 31.6 | 136.1 | 1.04 |
| C[e] | C4−$C_5$ | 81.6 | −12.7 | −68.9 | −5.6 | 131.7 | 1.37 |
| C[e] | C4−$C_6$ | 103.3 | 28.3 | −131.6 | 30.7 | 207.8 | 0.57 |
| 5′Me-C[e] | C4−$C_6$ | 102.9 | 19.6 | −122.5 | 24.9 | 197.4 | 0.68 |
| U[e] | U18−$C_5$ | 75.6 | −7.6 | −68.0 | −7.1 | 124.9 | 1.22 |
| U[e] | U18−$C_6$ | 113.3 | 11.7 | −125.0 | 28.7 | 207.1 | 0.81 |
| Me-A[f] | A20−$C_2$ | 90.0 | 0.0 | −90.0 | 3.5 | 155.9 | 1.00 |
| Me-A/Me-U[f] | A20−$C_2$ | 89.1 | 5.8 | −94.9 | 7.1 | 159.5 | 0.88 |

[a] The B3LYP functional with the 6-311++G** basis set was used in both geometry optimization and shielding tensor calculations. [b] Principal components given here refer to the traceless part of the CS tensor and were obtained from the calculated magnetic shielding tensor according to $\delta_{ii} = \sigma_{iso} - \sigma_{ii}$. [c] The angle $\theta$ is that between the $\delta_{XX}$ axis and the C−H bond, with the sign of $\theta$ defined just below eq 4. The angles between the geometry optimized C−H bond and the heavy atom bisector, used as a reference in the experimental results are 3.7° for dC−$C_6$, 3.9° for dT-$C_6$, 2.9° for A−$C_8$, 3.1° for G−$C_8$, 1.8° for C−$C_5$, 3.5° for C−$C_6$, 4.4° for 5′Me-C−$C_6$, −0.2° for U−$C_5$, 3.6° for U−$C_6$, 0.3° for A−$C_2$, and 1.0° for A−$C_2$/U, with the sign convention the same as for $\theta$. So, for example, for comparison to the experimental result for A−$C_8$, the above listed $\theta$ value needs to be decreased by 2.9°. [d] Coordinates taken from 1NAJ. [e] Coordinates taken from helix-35 (PDB 2GBH). [f] Coordinates taken from PDB entry 397D.[60]

## Discussion

The $^{13}C$ CSA parameters reported here have been extracted from double-helical RNA and DNA oligomers, using three different types of measurements: field dependence of the transverse relaxation rate, relaxation interference, and RCSA. For the RNA oligomer, which was uniformly enriched in $^{13}C$, slightly different experimental precautions were required relative to analogous measurements made on the DNA oligomer. Measurements were carried out with both Hahn-echo and spin-locked $T_{1\rho}$ experiments, and (with the exception of T−$C_6$) no systematic differences were found after the measured rates were corrected for the spin-flips of *J*-coupled passive spins (cf eq 1), which affect the two types of measurements differently. This result indicates that there are no substantial systematic errors in these measurements, and averaged values were used in the analysis.

For the DNA oligomer, CSA results are found to be in fair agreement with solid-state NMR results on DNA mononucleosides.[43] The largest difference between the solid-state NMR data and our results occurs for adenine $C_2$, where our results yield an 11% larger CSA magnitude and a smaller asymmetry. Likely, the increased CSA observed in our study results at least in part from the Watson−Crick base-pairing in the double-stranded helix. A−$C_2$ is located adjacent to $N_1$, which accepts an H-bond from U/T−$N_3$H. A comparison of results from quantum chemical calculations on an isolated adenine and a Watson−Crick A−U basepair (Table 2) also points to an increase in $C_2$ CSA upon H-bonding and a decrease in asymmetry.

Results for the other carbon types indicate a slightly (∼6%) larger CSA magnitude, $|\delta^M|$, for $C_5$ and $C_6$ than those of the solid-state NMR study, a smaller asymmetry of the $C_8$ CSA tensor, and slightly larger asymmetry for $C_6$. The asymmetries of the $C_5$ CSA tensor obtained by us and by Stueber and Grant differ substantially from the calculated value but agree reasonably well with one another.

In contrast to the asymmetry, the orientation of our experimental $C_5$ CSA tensor agrees well with computed results. For $C_8$, the results of Stueber and Grant and quantum calculations both suggest that the absolute value of the least-shielded principal CSA component is comparable to that of the most-shielded component (i.e., $|\delta_{XX}| \approx |\delta_{ZZ}|$), whereas our experimental results indicate that the most shielded component has the largest absolute value. The computed CSA tensors for G−$C_8$ and A−$C_8$ differ noticeably (Table 2). Therefore, we performed a joint fitting of the two tensors but forced the G−$C_8$ and A−$C_8$ $\eta$ and $\theta$ parameters to be the same, while each CSA magnitude is an independent variable. The best-fitted A−$C_8$ CSA magnitude exceeds G−$C_8$ CSA magnitude by 11 ppm. According to the *F* test statistics, the probability that the two CSA magnitudes are the same is 1.5%, indicating that the difference in CSA magnitudes is statistically significant. Analogous tests letting either $\eta$ or $\theta$ float did not result in significant differences.

Remarkably, we find that the $C_6$ CSA in A-form RNA is considerably larger than in B-form DNA. In a recent relaxation study of an RNA oligomer, Schwalbe and Duchardt[44] also noted that the literature values of $C_6$ CSA appeared incompatible with their relaxation measurements, and they suggested that an increase of 20 ppm in $|\delta^M|$ would be needed if dynamic behavior of base-paired pyrimidines and purines is assumed to be similar. Our RNA study indicates that the $C_6$ CSA exceeds the Stueber and Grant DNA values by about 30 ppm. The CSA magnitude, $|\delta^M|$, we observed for dC−$C_6$ in DNA is only 7 ppm larger than reported by Stueber and Grant. For dT−$C_6$, our experimental $|\delta^M|$ and $\theta$ values agree very well with those of Stueber and Grant, as well as those of Gregory et al.[87] The solid state $\eta$ values for C−$C_6$ fall between the values we observe for DNA and RNA. For dT−$C_6$, our $\eta$ value (1.02 ± 0.13) is smaller than those observed in the two solid-state NMR studies. However, considering the large experimental uncertainty in our $\eta$ value this difference does not appear to be significant.

Interestingly, quantum chemical calculations also show a significant increase in CSA for the RNA uridine and cytidine $C_6$ CSA over that of the DNA thymidine and cytidine values (Table 2). Inspection of the structure of A-form RNA nucleotides in both our NMR and high-resolution X-ray models indicates a possible explanation for the increased CSA observed in RNA. Specifically, in our NMR structure of helix35, the $C_6$H atoms are closer to the $O_5'$ oxygens ($r_{H-O} = 2.36 \pm 0.04$ Å) than the sum of the scaled van der Waals radii, suggesting a potential hydrogen-bonding type interaction. Atomic-resolution RNA X-ray structures (PDB codes 483D, 434D, 1QCU) with the H atoms added in an ideal geometry (in the base plane along the heavy atom bisector) using a 1.08 Å C−H distance, indicate even smaller distances between the $C_6$H and $O_5'$ atoms within the A-form (2.22 ± 0.09 Å). For comparison, average $C_6$H−$O_5'$ distances in B form DNA are 3.2 ± 0.2 Å. Interestingly, when the $C_6$ CSA tensor for the A-form RNA mononucleoside with $O_5'$ replaced by a hydrogen (i.e., generating a $C_5'$ methyl group) is computed, a 10 ppm reduction in the CSA magnitude is observed. However, this dependence on the precise location of nearby, nonbase atoms also suggests that pyrimidines that are not part of an A-form helical structure may have considerably smaller CSA values, complicating the quantitative analysis of relaxation data.

Differences in computed CSA values between RNA and DNA for nuclei other than pyrimidine $C_6$ are smaller (Supporting Information). With the relatively limited amount of available

(87) Gregory, D. M.; Mehta, M. A.; Shiels, J. C.; Drobny, G. P. *J. Chem. Phys.* **1997**, *107*, 28−42.

observables, we are unable to quantitatively confirm these smaller differences experimentally. Interestingly, RHF calculations systematically resulted in higher CSA magnitudes than B3LYP, by fractions ranging from 2 to 10%. Our experimental values are mostly bracketed by these two sets of results, with the exception of the pyrimidine $C_5$ CSA, where the calculated CSA magnitude is ca. 10−15% smaller than observed, and $|\delta_{XX}| > |\delta_{ZZ}|$, in contrast to the measurements which indicate $|\delta_{XX}| \approx |\delta_{ZZ}|$.

If it is assumed that the CS tensor for a given type of nucleus is independent of its location in the oligomer and has one of its principal components orthogonal to the plane of the base, the full tensor can be determined, at least in principle, from as few as three $\Delta\delta$ measurements. In this respect, it is interesting to note that the RCSA values provide the most direct information on the $^{13}C$ CSA tensor, as their interpretation only requires accurate knowledge of the molecular structure and the alignment tensor, which follow directly from prior extensive RDC measurements. Nevertheless, the minimum of $E^{\Delta\delta}(|\delta^M|,\eta,\theta)$ is relatively shallow, and this provided the main incentive to explore, in addition, relaxation measurements for defining the CS tensor. Analysis of the relaxation rates in terms of CS tensor parameters is considerably more involved than interpretation of $\Delta\delta$ values, as it relies on a diverse set of experiments and a relatively complex relation between the relative orientations of the molecular diffusion tensor, the CS tensor, and the dipolar interaction. Moreover, these relaxation rate measurements require particular precautions in terms of eliminating the effects of remote spins and $^{13}C-^{13}C$ $J$ modulation, as well as very accurate temperature calibration when studying the field dependence of relaxation on different spectrometers. However, in particular the results of relaxation interference experiments are highly discriminating when defining the angle (but not its sign) between the C−H bond vector and the least-shielded principal component of the CSA tensor, and therefore, they provide an important complement to the RCSA data. We note, however, that when only using the $\Delta\delta$ measurements to derive the CS tensor, best-fitted values fall close to those reported in Table 1, indicating that neither the $\Delta\delta$ values nor the relaxation data introduce a bias in the experimentally derived CSA parameters.

For proteins, there has been considerable discussion of the effect of motions on a time scale slower than the rotational diffusion on the observed dipolar couplings and how dipolar couplings potentially could reveal the presence of such motions.[19,88,89] Similarly, the presence of large amplitude domain motions in nucleic acids has been established from RDCs.[90] Our study focuses on individual, stable, double-stranded helical segments. Hydrogen-exchange protection factors for the imino protons, measured in these oligonucleotides, are above 50 for all nonterminal basepairs, indicating that Watson−Crick base pairing remains intact for at least 98% of the time. This suggests that large amplitude motions associated with base pair opening are relatively rare events that therefore should have minimal impact on the analysis of the measured $\Delta\delta$ values. However, if large axial fluctuations of intact basepairs around the helical axis were present, not precluded by the high protection factors, it can be shown that to first order these have very little impact on the derived CSA values (Supporting Information).

## Concluding Remarks

Next to CSA magnitude and asymmetry, our study provides experimental information on the $x$ and $y$ component orientation of the CSA tensors of protonated carbons in the nucleotide base planes of double-helical DNA and RNA and indicates fair agreement with results from quantum chemical calculations. Results presented by Stueber and Grant[43] showed a considerable dependence of both the $\eta$ value and the orientation of the $x$ and $y$ components on the electrostatic crystal potential. Differences between the CSA values applicable for Watson−Crick base-paired oligonucleotides, observed in our study, and for the mononucleotides studied by solid-state NMR therefore are not surprising. Except for the requirement to prepare identical buffer conditions for aligned and isotropic samples used, precise measurement of base RCSA is simple and sensitive. With accurate knowledge of the applicable $^{13}C$ CSA tensors in hand, RCSA measurement now provides an attractive complement to measuring RDCs. Because the base carbon CSA tensors are highly asymmetric, with the pseudounique principal component aligned orthogonal to the base plane, and the dipolar $^{13}C-^{1}H$ interaction is axially symmetric and in the base plane, the RCSA and RDC values are highly complementary and together can lift the degeneracy in base orientation associated with each individual type of measurement.

**Acknowledgment.** We thank Dennis Torchia (NIDCR, NIH) for valuable discussions and Nico Tjandra and Shou-Lin Chang (NHLBI, NIH) for a copy of their program to calculate relaxation rates for an anisotropic rotor. The RNA sample used in this study was kindly provided by Ed Nikonowicz and Izabela Tworowska (Rice University). This work was supported by the Intramural Research Program of the NIDDK, NIH, and by the Intramural Antiviral Target Program of the Office of the Director, NIH. D.L.B. thanks NSERC for continued support.

**Supporting Information Available:** Full ref 59, one table containing the experimentally observed parameters for the RNA oligomer, one analogous table for the DNA oligomer, one table with the base CSA parameters obtained from best-fitting and from jack-knife cross validation, one table with jack-knifed cross validation statistics, one table with computed (B3LYP and RHF) shielding tensors for various nucleotides, one table with best-fitted rotational diffusion tensor orientations for the RNA oligomer, when separately fitting the $C_2$, $C_5$, $C_6$ and $C_8$ experimental data, one table with best-fitted alignment tensors when using an ensemble of structures, one table with best-fitted CSA data when using an ensemble of structures, one table with best-fitted CSA data when assuming a uniform 1 Hz $R_{ex}$ contribution, one table with CSA parameters when best-fitting using a range of $D_{\parallel}/D_{\perp}$ values, one figure showing the error surface for the fitted parameters as a function of $|\delta^M|$, $\eta$, and $\theta$, one figure showing the error surface for $dC-C_6$ when $\theta$ is fixed at 28°, and one figure showing the error in the fit as a function of RNA diffusion anisotropy. This material is available free of charge via the Internet at http://pubs.acs.org.

JA061984G

(88) Meiler, J.; Prompers, J. J.; Peti, W.; Griesinger, C.; Bruschweiler, R. *J. Am. Chem. Soc.* **2001**, *123*, 6098−6107.
(89) Bouvignies, G.; Bernado, P.; Meier, S.; Cho, K.; Grzesiek, S.; Bruschweiler, R.; Blackledge, M. *Proc. Natl. Acad. Sci. U.S.A.* **2005**, *102*, 13885−13890.
(90) Al-Hashimi, H. M.; Gosser, Y.; Gorin, A.; Hu, W. D.; Majumdar, A.; Patel, D. J. *J. Mol. Biol.* **2002**, *315*, 95−102.